

Measurement and Calculation of the Rate Constant for the Reaction of Isopropyl Isocyanate with Hydroxyl Radical

JAMES K. PARKER,¹ CYNTHIA ESPADA-JALLAD,¹ CLAUDIA L. PARKER,² JOHN D. WITT¹

¹Chemical Detection Division, Midwest Research Institute, Kansas City, MO 64110

²Department of Chemistry, Rockhurst University, Kansas City, MO 64110

Received 17 December 2007; revised 4 April 2008, 8 August 2008; accepted 28 August 2008

DOI 10.1002/kin.20390

Published online in Wiley InterScience (www.interscience.wiley.com).

ABSTRACT: The rate constant for the gas-phase reaction of hydroxyl radical with isopropyl isocyanate (IIC) has been measured, relative to toluene, in the $T = 287\text{--}321$ K range at atmospheric pressure in air. Ultraviolet photolysis of methyl nitrite served as the source of hydroxyl radical. The experimental Arrhenius expression obtained for this reaction is $7.09 \times 10^{-13} \times \exp[(307 \pm 263)/T]$ $\text{cm}^3 \text{ molecule}^{-1} \text{ s}^{-1}$, where the indicated error is one least-squares standard deviation and does not include the uncertainty in the rate constant for toluene. Multilevel ab initio calculations, performed at the MP-SAC2 level, indicate that hydrogen atom transfer from the tertiary carbon atom occurs without an energy barrier, in agreement with the experimentally observed slight negative temperature dependence of the rate constant. The calculations indicate that hydrogen-bonded complexes of IIC and OH form in the reactant entrance channels along the minimum-energy paths. Use of conventional transition state theory and MP-SAC2 scaled transition state relative energies, with an asymmetric Eckart tunneling model for transfer of a hydrogen atom from a methyl group, yields a theoretical rate constant of $1.81 \times 10^{-18} \times T^2 \times \exp(744/T)$ $\text{cm}^3 \text{ molecule}^{-1} \text{ s}^{-1}$ in the $T = 200\text{--}350$ K range. From the rate constant data, an estimated upper limit for the tropospheric lifetime of IIC is determined as 6.0 days at 15°C, based on the global weighted-average OH concentration of 9.4×10^5 molecules cm^{-3} determined by Prinn et al. (*Science* 2001, 292, 1882–1888). © 2008 Wiley Periodicals, Inc. *Int J Chem Kinet* 41: 187–197, 2009

Correspondence to: James K. Parker; e-mail: jparker@mrresearch.org

Supporting information containing tables with equilibrium geometries, vibrational frequencies, and rotational constants for all species listed in Table II is available in the online issue at www.interscience.wiley.com.

© 2008 Wiley Periodicals, Inc.

INTRODUCTION

Toxic industrial chemicals (TICs) are routinely used throughout the world to manufacture insecticides, herbicides, plastics, foams, and other high-tech materials required by society [1]. In 1998, the NATO International Task Force-25 created the TIC Hazard List, a

compilation of the top 100 toxic chemicals used by the industry [2]. The Hazard List rankings are determined according to the chemical's production, transport, storage, toxicity, and vapor pressure. Release of large quantities of these chemicals into the troposphere, either accidental or intentional, is of concern due to their toxicity. For example, the compound methyl isocyanate (MIC), an acute toxin even at low concentration [2], was accidentally released from a Union Carbide chemical plant in Bhopal, India, in 1984 resulting in approximately 2000 fatalities and 50,000 injuries; a total of 320,000 people were estimated to have been exposed [3].

This paper focuses on experimental measurement of the rate constant for reaction of isopropyl isocyanate (IIC) with hydroxyl radical. In addition, *ab initio* calculations are presented to provide insight into the reaction mechanism and to estimate the value of the rate constant at conditions outside of the experiments. To date, there has been no published study for reaction of any organic isocyanate with hydroxyl radical. Because of the lack of such data, and to form an understanding of the chemical reaction dynamics for reaction of organic isocyanates with hydroxyl radical, we have undertaken a combined experimental and theoretical study of the kinetics for the IIC + OH reaction.

Like MIC, IIC is also listed on the TIC Hazard List. IIC is a clear, colorless liquid at ambient conditions. It reacts exothermically with water and has a boiling point of 74°C. The results of this study form a basis for understanding the atmospheric fate of IIC. We present here the results of relative rate experiments for the reaction of IIC with hydroxyl radical in the $T = 287\text{--}321$ K range. Additional insight into the reaction mechanism has been gained from *ab initio* electronic structure calculations. The results of the electronic structure calculations have been used to compute the rate constant from conventional transition state theory (TST) in the $T = 200\text{--}350$ K range. This allows for an extrapolation of the experimental data over the entire range of temperature accessible in the troposphere. Although this paper focuses only on loss of IIC to reaction with hydroxyl radical, in the atmosphere there is the possibility of other losses including, but not limited to, reactions with NO_3 and O_3 , photolysis, and dry/wet deposition.

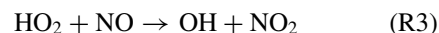
EXPERIMENTAL AND COMPUTATIONAL METHODS

The rate constant for the title reaction was measured using a relative rate technique [4] in the $T = 287\text{--}321$ K range at $P = 740 \pm 10$ Torr of purified air. Toluene was chosen as the reference compound because its rate

constant for reaction with hydroxyl radical is similar in magnitude to that of IIC and it has been extensively studied [5–11]. The reaction chamber consisted of a FEP Teflon collapsible bag of 0.13-mm thickness and 220 L in volume surrounded by 16 40-W fluorescent black lamps with $\lambda_{\text{max}} = 350$ nm (Sylvania F40/350 BL). This bag and associated lighting was placed in a completely dark cabinet to exclude unwanted light. During irradiations only 8 of the lamps were turned on to minimize temperature variations in the chamber. Temperature control was achieved by a flow of $1.7 \text{ m}^3 \text{ min}^{-1}$ thermostated air through the insulated cabinet. Temperatures were recorded at positions just above and below the bag with calibrated T-type thermocouples. The experimental uncertainty in temperature is ± 1 K.

Mixtures of IIC–toluene–NO– CH_3ONO –air were made up under the flow of 5.0 standard liters per minute of purified air (Aadco zero air generator, model 737; Aadco, Cleves, OH). According to the zero air generator manufacturer's specifications, the purified air quality was such that there was less than 1 ppb ozone, methane, hydrocarbons, NO_x , H_2S , SO_2 , COS, CO, CO_2 , SF_6 , and fluorocarbons; the dew point of the purified air did not exceed -51°C ; and oxygen was a constant 21% of the mixture. Approximately $0.15 \mu\text{L}$ of liquid IIC (Sigma-Aldrich, St. Louis, MO; $\geq 98\%$), $0.20 \mu\text{L}$ of liquid toluene (Sigma-Aldrich, 99.8%), 2.4 cm^3 methyl nitrite (Midwest Research Institute, Kansas City, MO; 99.5+%), and 2.4 cm^3 nitric oxide (Linde, Murray Hill, NJ; 99.5%), diluted to 10 cm^3 with argon (Nitrogen Air Pressure Co., Olathe, KS; 99.999%) to suppress its oxidation upon introduction into the air stream, were injected under the flow of purified air into a 1/4-in.-inside-diameter silco-coated steel line (Restek, Bellefonte, PA) via a tee capped at the middle port with a septum. The initial gas-phase concentrations of the reactants were set to $[\text{toluene}]_0 = 150$ ppb; $[\text{IIC}]_0 = 150$ ppb; $[\text{NO}]_0 = 11$ ppm; and $[\text{CH}_3\text{ONO}]_0 = 11$ ppm.

Hydroxyl radicals were generated by the UV-photolysis of methyl nitrite in air [4,12]:



The reaction was carried out in excess nitric oxide to suppress formation of ozone. The concentrations of NO and NO_2 were measured periodically with a chemiluminescence analyzer (Thermo Electron, Waltham, MA; model 42i). The initially measured NO concentration (after the mixtures have been prepared but before any photolysis) was found to be approximately

4 ppm 2 h after preparation of the mixtures. About 60% of the NO was oxidized upon introduction of the 24% NO/76% Ar mixture into the flow of purified air.

The concentrations of IIC and toluene were followed by gas chromatography (Hewlett Packard, Santa Clara, CA; G1530A) with electron-ionization mass spectrometric detection (Agilent, Santa Clara, CA; 5975 MSD) at $m/z = 70$ for IIC and $m/z = 91$ for toluene. For the analyses, gas samples of 100 cm³ volume were collected from the reaction chamber with the aid of a mass flow meter and digital stopwatch onto Chromosorb-106 solid adsorbent. IIC and toluene reactants were desorbed from the Chromosorb-106 in a two-stage method. The first stage of the thermal desorption heats the Chromosorb-106 to 190°C at a helium carrier gas flow of 50 standard cubic centimeters per minute and deposits the analytes onto a Tenax-TA cold trap held at -5°C. In the focusing stage, the cold trap is flash heated to 270°C (in about 3 s) under a flow of He and the analytes are deposited onto a 5% diphenyl/95% dimethyl polysiloxane column (Restek, model Rtx-5MS, 15 m × 0.25 mm, 1 μm) held at 20°C for 1.0 min and temperature programmed to 120°C at 10°C min⁻¹. Analytical uncertainties were estimated from replicate analyses in the dark and were typically 4%–5% for both toluene and IIC.

Quantum mechanical calculations were carried out using the software program GAMESS [13]. Initially, geometry optimizations to local minima and first-order saddle points were obtained at the unrestricted HF/6-31G(d) level of theory for doublet states [14–29]. The spin contamination in these wave functions was minor, with $\langle S^2 \rangle \leq 0.784$ for all stationary points. These Hartree–Fock equilibrium structures were then used as starting points for geometry optimizations at the UMP2/6-31G(d) level of theory [30]. One hydrogen-bonded complex, species **5**, could not be located at the UHF/6-31G(d) level of theory; its equilibrium structure was found at UMP2/6-31G(d) only. Local minima Hessians were obtained by single numerical differentiation (default) with a threshold for gradient convergence of 10⁻⁴ hartree bohr⁻¹ (default); saddle point Hessians were obtained by double numerical differentiation with a threshold for gradient convergence of 10⁻⁵ hartree bohr⁻¹. The tighter convergence criteria and double differentiation for saddle points were used to reduce errors in finite differencing. This resulted in all of the translational and rotational modes of the transition states being calculated as real modes and not erroneously as imaginary modes. In the search for first-order saddle points, the Hessian matrix was numerically computed at every step. Zero-point vibrational energies (ZPVE) are listed for the level of theory at which they are evaluated. Single-point en-

ergies were evaluated with second-order perturbation theory using the 6-311++G(2d,p) basis set [31–34]. And finally, MP-SAC2 energies were obtained from the MP2/6-311++G(2d,p) single-point energies using the method of Gordon and Truhlar [35] and Lynch and Truhlar [36]. MP-SAC2 ZPVEs are obtained by scaling the HF/6-31G(d) and MP2/6-31G(d) ZPVEs according to Eq. (1).

Tuong and Truhlar have shown the MP-SAC2 method yields good agreement between TST and experimental rate constants for the OH + CH₄ reaction over a very wide temperature range [37,38]. Moreover, Truhlar et al. have shown that multilevel ab initio calculations in general are far superior to the most advanced single level ab initio calculation on which they are based for computing properties such as barrier heights, which are essential for rate constant calculations [36,39,40]. For example, the mean error in computing 44 reaction barrier heights is +12 kJ mol⁻¹ for the MP-SAC2 method versus +19 kJ mol⁻¹ for the pure MP2/6-311++G(2d,p) ab initio method [36].

The MP-SAC2 method, more generally known as MP-SAC_{*n*} and termed scaling all correlation energy, is a correction scheme designed to extrapolate single determinant many-body perturbation theory calculations to the full CI-limit and the complete one-electron-basis-set limit in a single step [35]. It is an implicit extrapolation scheme in that it relies on the assumption that errors are constant across a potential energy surface. The scaling all correlation energy obtained by second-order perturbation theory is given as

$$E_{\text{MP-SAC2}} = E_{\text{SCF}} + \frac{E_{\text{MP2}} - E_{\text{SCF}}}{F_2} \quad (1)$$

The MP-SAC2 method was chosen for this work because all calculations involving this molecular system could be carried out on an IBM-compatible personal computer with one Pentium IV chip and 1 GB of RAM. The single empirical parameter, F_2 , accounts for both the incomplete correlation treatment and the basis set deficiencies of the MP2/6-311++G(2d,p) calculation.

For results of this paper, the E_{MP2} values are the ZPVE-corrected single-point energies calculated at the MP2/6-311++G(2d,p) level of theory using the MP2/6-31G(d) equilibrium structures. E_{SCF} values are the ZPVE-corrected single-point Hartree–Fock energies obtained from the MP2/6-311++G(2d,p) results (i.e., they are based on MP2/6-31G(d) optimizations). The scaling factor, F_2 , is a constant that depends on the basis set employed and the specific type of bond

studied. F_2 is defined as

$$F_2 = \frac{D_e(\text{MP2}) - D_e(\text{SCF})}{D_e(\text{expt}) - D_e(\text{SCF})} \quad (2)$$

where D_e refers to the bond energy as obtained from experiment, a self-consistent field (SCF) calculation, or second-order perturbation theory. For the 6-311++G(2d,p) basis set, the F_2 value used in this work is 0.878 and is a composite based on the C–H and O–H bond energies of CH₄ and H₂O [35]. The scaling factor used in determination of the MP-SAC2 ZPVEs is specific to the 6-31G(d) basis set and has a value of 0.665 for the C–H/O–H system.

Conventional TST was used to calculate rate constants for the reaction channels [41–43]. The reaction rate constant was computed with the following TST expression:

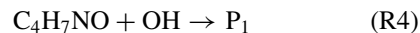
$$k(T) = \Gamma \frac{k_B T}{h} \frac{Q^{\text{TS}}}{Q^{\text{OH}} Q^{\text{R}}} \exp\left(\frac{-\Delta E_0}{k_B T}\right) \quad (3)$$

In Eq. (3), Γ is a one-dimensional asymmetrical Eckart tunneling correction [44]; Q^{TS} , Q^{OH} , and Q^{R} are the transition state, OH radical, and IIC reactant total partition functions, calculated via the rigid rotor-harmonic oscillator approximation [45] at temperature T ; ΔE_0 is the computed barrier height at the saddle point and includes the ZPVE correction; k_B is Boltzmann's constant; and h is Planck's constant. All vibrational modes were scaled according to the recommendation of Merric et al. [46] prior to computing values of the vibrational partition functions. The accuracy of rate constants computed with Eq. (3) is limited primarily by the accuracy of ΔE_0 [43]. A well-known systematic error in ab initio calculations is that they tend to overestimate barrier heights while hybrid density functional calculations tend to underestimate them [36,47]. Attainment of an accurate value for ΔE_0 is the motivation for use of multilevel ab initio calculations in this work.

RESULTS AND DISCUSSION

When purified air mixtures containing 0.5 ppm IIC, 0.5 ppm toluene, and 0.5 ppm isoprene as an OH radical sink ($k_{(\text{isoprene}+\text{OH})} = 1.0 \times 10^{-10} \text{ cm}^3 \text{ molecule}^{-1} \text{ s}^{-1}$ at $T = 298 \text{ K}$) [48] were subjected to radiation from eight lamps for 30 min, no losses for any compound were observed. Irradiation times for all rate constant experiments were 15–20 min. No dark losses were observed when an IIC–toluene–air mixture (0.5 ppm in each reagent) was allowed to stand undisturbed for a 17-h period.

When methyl nitrite and nitric oxide are added to the mixture at 11 ppm concentration and the UV lights are switched on, the reactions that contribute to loss of IIC (C₄H₇NO) and toluene (C₇H₈) are as follows:



The relative rate equation, which relates the concentrations of IIC and toluene to the rate constants k_4 and k_5 , is [4]

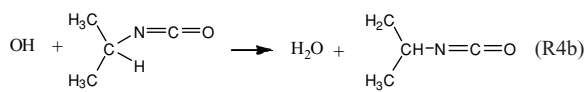
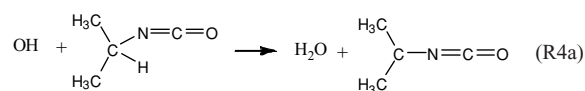
$$\ln \left\{ \frac{[\text{C}_4\text{H}_7\text{NO}]_0}{[\text{C}_4\text{H}_7\text{NO}]_t} \right\} = \frac{k_4}{k_5} \ln \left\{ \frac{[\text{C}_7\text{H}_8]_0}{[\text{C}_7\text{H}_8]_t} \right\} \quad (4)$$

In Eq. (4), $[\text{C}_4\text{H}_7\text{NO}]_0$ is the concentration of IIC before irradiation at time $t = 0$, $[\text{C}_4\text{H}_7\text{NO}]_t$ is the concentration of IIC at time t , $[\text{C}_7\text{H}_8]_0$ is the concentration of toluene at $t = 0$, and $[\text{C}_7\text{H}_8]_t$ is the concentration of toluene at time t . Note that time does not explicitly appear in Eq. (4). Also, Eq. (4) is strictly valid when losses of C₄H₇NO and C₇H₈ are due only to reaction with OH radical. When the data are plotted according to Eq. (4), the slope of the linear regression line is equal to the rate constant ratio k_4/k_5 and the intercept is zero. Representative data obtained at $T = 296 \pm 1 \text{ K}$ are plotted in Fig. 1. All quoted experimental uncertainties for rate constant ratios and rate constants are derived from the relative rate plots at the two-sigma level and are statistical only.

The data of Fig. 1 yield a rate constant ratio $k_4/k_5 = 0.329 \pm 0.030$. Rate constant k_4 is placed on an absolute basis by use of $k_5 = 1.81 \times 10^{-12} \exp(338 \text{ K}/T) \text{ cm}^3 \text{ molecule}^{-1} \text{ s}^{-1}$ [5]. The resulting value of k_4 is $(18.7 \pm 1.8) \times 10^{-13} \text{ cm}^3 \text{ molecule}^{-1} \text{ s}^{-1}$. Table I lists the values of the rate constant ratios (k_4/k_5) and the associated rate constants (k_4) obtained in this work.

The data of Table I are plotted in Arrhenius form in Fig. 2.

The relative rate experiment measures the total rate constant for reaction R4. There are two distinct pathways available to this reaction:



Channel 4a is expected to be the dominant reaction channel as it leads to formation of a relatively stable

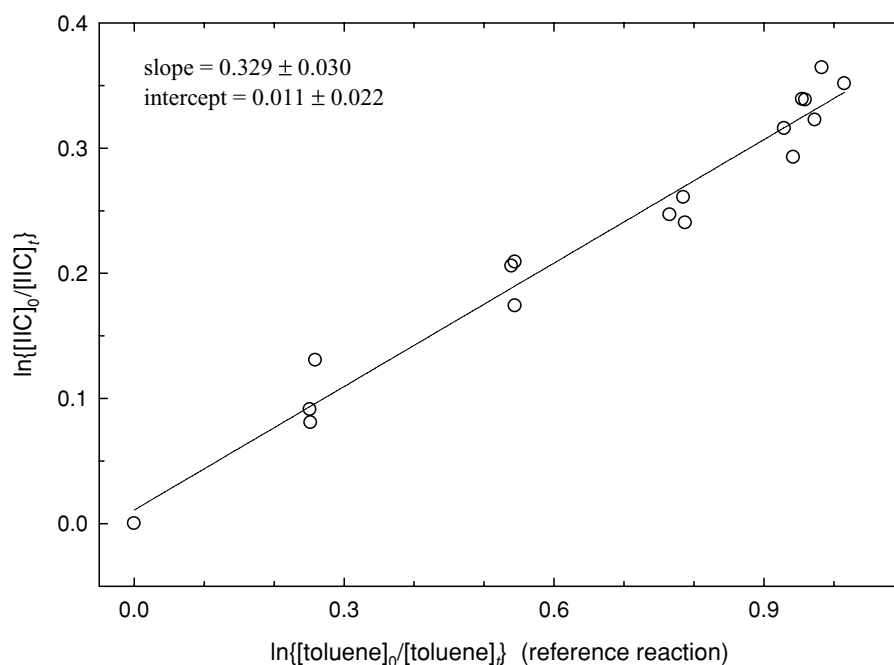


Figure 1 Plot of the data at $T = 296$ K and $P = 737$ Torr according to Eq. (4). The slope of the linear regression line is $k_4/k_5 = 0.329 \pm 0.030$.

tertiary radical, while channel 4b leads to formation of a primary carbon radical. A structure-reactivity model (SAR) known as the Atmospheric Oxidation Program [49–51], an empirical algorithm designed to estimate the OH rate constant for organics, predicts a total rate constant for R4 of $22.7 \times 10^{-13} \text{ cm}^3 \text{ molecule}^{-1} \text{ s}^{-1}$ at $T = 298$ K with 85.5% of the reaction occurring through R4a. Considering that SAR is an empirical estimate of the rate constant, the level of agreement with our experimental result is very good. The SAR rate constant is 15% larger than the experimental value obtained from Fig. 2 at $T = 298$ K.

Table I Rate Constant Ratios, k_4/k_5 , and Rate Constants, k_4 ($\text{cm}^3 \text{ molecule}^{-1} \text{ s}^{-1}$), for the Reaction of OH Radical with Isopropyl Isocyanate in the Range $T = 287\text{--}321$ K

T (K)	k_4/k_5	$10^{13} \times k_4^a$
287	0.373 ± 0.060	21.9 ± 3.5
290	0.337 ± 0.020	19.5 ± 1.2
294	0.386 ± 0.044	22.1 ± 2.6
296	0.329 ± 0.030	18.7 ± 1.8
300	0.313 ± 0.056	17.5 ± 3.2
305	0.359 ± 0.024	19.7 ± 1.4
309	0.389 ± 0.024	21.0 ± 1.3
315	0.316 ± 0.020	16.7 ± 1.1
321	0.395 ± 0.032	19.9 ± 1.6

^aPlaced on an absolute basis by use of $k_5 = 1.81 \times 10^{-12} \exp(338/T) \text{ cm}^3 \text{ molecule}^{-1} \text{ s}^{-1}$ [5].

Figure 3 presents pictorial views [52] of reactants, transition states (TS1 and TS2 are both first-order saddle points on the minimum energy path or MEP), and complexes involved in reaction R4. Table II presents relative energies of all stationary point species, including products. Figure 4 is an energy level diagram that highlights the stationary points occurring on the MEPs for reaction channels 4a and 4b. Tables of supporting information (III–XXV) give the absolute electronic energies and ZPVEs for those species listed in Table II, as well as equilibrium Cartesian coordinates, vibrational frequencies, and rotational constants for all stationary point species participating in reaction R4.

Two isomers of IIC, structures **1** and **2**, which differ by rotation about the C–N single bond, were found to be local minima on the MP2/6-31G(d) potential energy surface. They are very close in energy, separated by only $0.281 \text{ kJ mol}^{-1}$ at the MP-SAC2 level. Also shown in Fig. 3 are transition states corresponding to reactions R4a and R4b, structures **TS1** and **TS2**, respectively. **TS1** is a *submerged* first-order saddle point as it lies below the energy of separated reactants, with a relative energy of $-1.16 \text{ kJ mol}^{-1}$ with respect to reactants **2** + OH at the MP-SAC2 level of theory.

The reaction pathways are shown in the diagram of Fig. 4. Both pathways that lead to R4a and R4b products are of the addition/decomposition type. Conformer **1** of IIC and OH form hydrogen-bonded complex **4**, which is connected to **TS2** and the products of R4b. Conformer **2** of IIC and OH form hydrogen-bonded

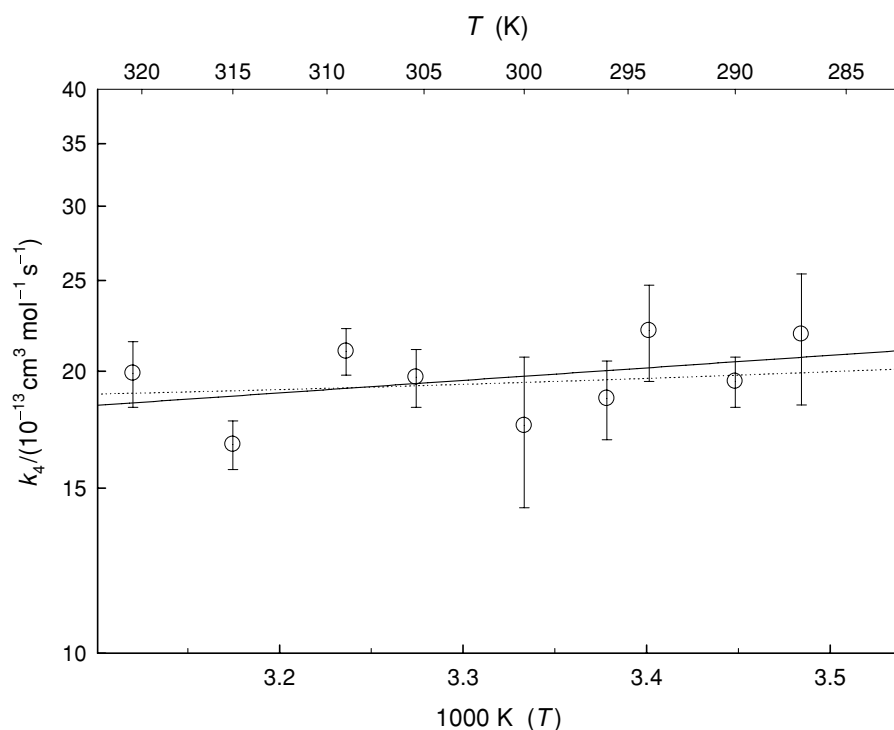


Figure 2 Arrhenius plot of k_4 in the range $T = 287\text{--}321$ K. The equation of the solid regression line is $k_4 = 7.09 \times 10^{-13} \times \exp[(307 \pm 263)/T] \text{ cm}^3 \text{ molecule}^{-1} \text{ s}^{-1}$. The error bars represent two-sigma standard deviation of the slopes of the relative rate plots. The dotted line represents TST rate constants calculated for the two channels and is given by $k_4(\text{TST}) = 1.81 \times 10^{-18} \times T^2 \times \exp(744/T) \text{ cm}^3 \text{ molecule}^{-1} \text{ s}^{-1}$, for $T = 200\text{--}350$ K.

complex **5**, which is connected to **TS1** and the products of R4a. Intrinsic reaction coordinate calculations (IRC) [53], carried out at the MP2/6-31G(d) level, reveal that **TS1** is connected directly to Complex **5** and R4a products (3°C radical) on the MEP. We have also verified that **2** can form Complex **3** with OH radical. Complex **3** is a hydrogen-bonded adduct of OH radical and IIC with the nitrogen atom of IIC acting as the hydrogen bond acceptor. Once formed, Complex **3** can dissociate back to reactants; no pathway on the MEP was found for Complex **3** to proceed to products. Nevertheless, a qualitative look at Complex **3** suggests that decomposition of the complex to R4a products (3° radical and water) should be feasible.

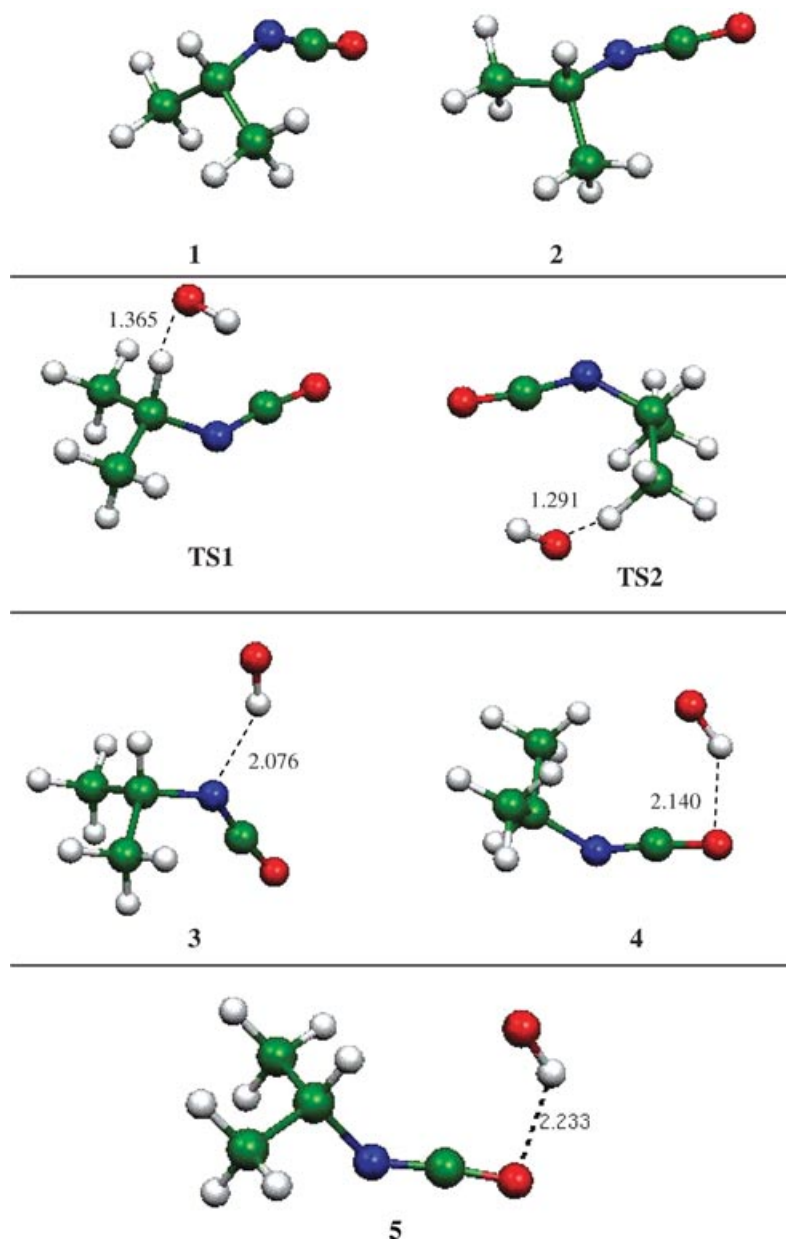
Isomer **1** of IIC and OH form Complex **4** with relative energy of $-13.3 \text{ kJ mol}^{-1}$ at the entrance channel of R4b. Complex **4** is a hydrogen-bonded adduct of IIC and OH with the oxygen atom of IIC acting as the hydrogen bond acceptor. This complex, like **3**, is in a relatively shallow well on the MEP. Once formed Complex **4** can either dissociate back to **1** and OH or proceed through **TS2**, as verified by IRC calculation, to form R4b products (1°C radical). It is interesting to note that IIC can form hydrogen-bonded complexes with OH at the reaction entrance channels. This type

of behavior has been observed for reactions of oxygenated hydrocarbons, in particular ketones, aldehydes, and carboxylic acids, with OH radical [54]. In summary, it appears that IIC reacts with OH radical in a complex-forming/decomposition mechanism under conditions relevant to the troposphere. It is possible that at low temperatures ($T < 200$ K), Complexes **3**, **4**, and **5** may be collisionally stabilized and exert a noticeable influence on the rate of reaction. Addition of OH to the NCO system in the molecule is not expected to be an energetically available pathway and was not considered in the ab initio calculations.

Conventional TST rate constants, calculated using the MP-SAC2 relative energies of saddle points listed in Table II, produce rate constants that are a factor of 2.4 lower than experiment. The largest source of error in a TST calculation is typically the determination of the barrier height, since this occurs in the exponential factor of Eq. (3). Another potential source of error is in the calculation of the partition functions. One measure of the reliability of the RR-HO approximation [45] for calculating partition functions is a comparison of theoretical and experimental A-factors. The TST A-factor at $T = 300$ K, a composite value weighted according to the branching fractions for **TS1** and **TS2** (see Eq. (5)),

Table II Relative Energies (kJ mol^{-1}) at $T = 0$ K of Species in Fig. 4 Optimized at the MP2/6-31G(d) Level

Species	MP2/6-31G(d)	MP2/6-311G++(2d,p)	MP-SAC2
1 + OH	0.00	0.00	0.00
2 + OH	+1.05	+0.195	+0.281
TS1	+21.0	+8.58	-0.874
TS2	+32.3	+19.9	+9.76
3	-17.1	-11.4	-12.5
4	-21.0	-12.3	-13.3
5	-16.8	-10.2	-12.0
R4a products	-82.1	-107.5	-115.4
R4b products	-41.1	-69.9	-77.9

**Figure 3** Pictorial representations of equilibrium MP2/6-31G(d) structures of species important in the reaction of OH radicals with IIC. Numbers next to dashed lines indicate interatomic distances (angstroms). Carbon atoms are green, hydrogen atoms are white, oxygen atoms are red, and nitrogen atoms are blue. [Color figure can be viewed in the online issue, which is available at www.interscience.wiley.com.]

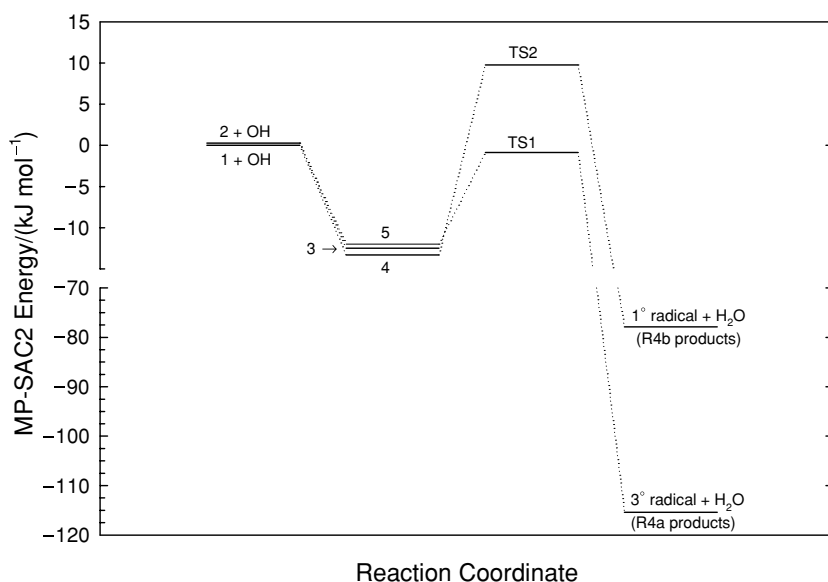


Figure 4 Energy level diagram for the reaction of IIC with hydroxyl radical. Conformer **2** combines with OH radical to form Complex **3**, which can dissociate to reform **2** + OH; Conformer **2** and OH can react through subthreshold saddle point **TS1** ($-1.16 \text{ kJ mol}^{-1}$) via Complex **5** to form R4a products. Conformer **1** and OH radical form Complex **4** at the entrance channel that can dissociate or proceed through a positive barrier at **TS2** ($+9.76 \text{ kJ mol}^{-1}$) to form R4b products.

is $6.4 \times 10^{-13} \text{ cm}^3 \text{ molecule}^{-1} \text{ s}^{-1}$; this compares favorably with the experimental value of $7.1 \times 10^{-13} \text{ cm}^3 \text{ molecule}^{-1} \text{ s}^{-1}$, suggesting that RR-HO is a reasonable approximation in this temperature range. Also, we tested the applicability of RR-HO for some low-frequency bond torsion modes in the reactants and transition state. Specifically, we calculated barrier heights to internal rotation of methyl groups, both in IIC and in **TS1**, and for internal rotation of the OH group in **TS1**. We found that the barrier heights for these internal rotations are significantly higher than $k_B T$ in the experimental range of temperatures. These results confirm that RR-HO is appropriate for these modes [55].

Ideally, the TST rate constants would be of such quality that an extrapolation of the experimental data could be made to cover the whole range of temperatures available in the troposphere. Toward this end, we have lowered the relative energies of both **TS1** and **TS2** by 2.37 kJ mol^{-1} to obtain good agreement between theory and experiment in the temperature range of the experimental study (Fig. 2). The lowering of both transition state energies by the same amount is consistent with the assumption of SAC that errors are constant across a potential energy surface [35]. The lowering of the barrier heights by 2.37 kJ mol^{-1} is well within the estimated 12 kJ mol^{-1} uncertainty of the MP-SAC2 method [36]. We note that $\Delta G^{\ddagger}(\text{TS1})$ is expected to remain positive for temperatures greater than 30 K even though $\Delta E^{\ddagger}(\text{TS1})$ is negative (value of -3.52 kJ

mol^{-1} used in calculation of TST rate constants); the value of $\Delta S^{\ddagger}(\text{TS1})$ is $-114.9 \text{ J mol}^{-1} \text{ K}^{-1}$ from the MP2/6-31G(d) stationary point calculations.

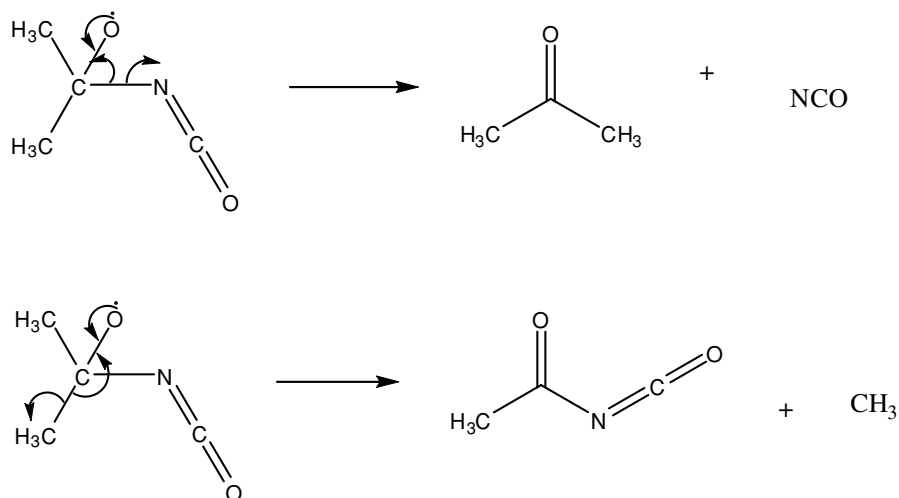
One-dimensional Eckart tunneling factors were obtained for channel 4b with the relative energy of **TS2** set to 7.39 kJ mol^{-1} . The Eckart barrier was defined for reaction of Complex **4** through **TS2** to R4b products. Tunneling factors varied from 58.3 at $T = 200 \text{ K}$ to 3.75 at $T = 350 \text{ K}$. A statistical factor of six was applied for channel 4b rate constants to account for the six hydrogen atoms of the two methyl groups. No tunneling correction was included for channel 4a since there is no barrier on the MEP. The total TST rate constant is described by $k_4(\text{TST}) = 1.81 \times 10^{-18} \times T^2 \times \exp(744/T) \text{ cm}^3 \text{ molecule}^{-1} \text{ s}^{-1}$, for $T = 200\text{--}350 \text{ K}$. This function is plotted as the dotted line of Fig. 2. The main reaction channel, R4a, is described by $k_{4a}(\text{TST}) = 1.75 \times 10^{-18} \times T^2 \times \exp(733/T) \text{ cm}^3 \text{ molecule}^{-1} \text{ s}^{-1}$. Division of k_{4a} by k_4 yields a nearly temperature-independent branching fraction, β , for 4a:

$$\beta = \frac{k_{4a}}{k_{4a} + k_{4b}} = 0.967 \times \exp(-11/T) \quad (5)$$

$T = 200\text{--}350 \text{ K}$

At $T = 298 \text{ K}$, β has a value of 0.932; the SAR model predicts a branching fraction of 0.855 for channel R4a at this temperature.

One experiment, designed to identify and measure the yields of products of R4, was conducted



Scheme 1 Possible bond fission stabilization pathways of the initially formed alkoxy radical in air with excess nitric oxide.

with $[\text{IIC}]_0 = 2.0$ ppm, $[\text{NO}]_0 = 4$ ppm, $[\text{CH}_3\text{ONO}]_0 = 11$ ppm in purified air at $T = 299$ K and $P = 740$ Torr. Aliquots of 100 cm^3 were sampled at $t = 0$ and at various times up to $t = 1200$ s when $[\text{IIC}]_{1200} = 1.2$ ppm. Samples were desorbed onto the GC column and detected by mass spectrometry in the same manner as for the kinetics runs. The detection sensitivity of the MS is about 10 ppb for most analytes when 100 cm^3 of gas is sampled ($S/N \approx 1$). The expected S/N ratio for stoichiometric conversion of IIC to products would be about 80, based on converting 0.8 ppm of IIC to a primary product of R4, which reacts slowly (as compared to IIC) with OH.

We expected that acetone, with an OH rate constant of $1.7 \times 10^{-13}\text{ cm}^3\text{ molecule}^{-1}\text{ s}^{-1}$ [48], would be a product of R4 based on model chemistry of simple organic compounds with OH radical in air in the presence of nitric oxide [56]. Scheme 1 shows two possible stabilization pathways of the alkoxy radical, formed by reactions of the R4a radical product with oxygen in excess nitric oxide.

No acetone was observed within the uncertainty of the GC-MS measurements. That acetone is not a primary product of reaction R4 in air is surprising; it is possible that the $(\text{CH}_3)_2\text{C}(\text{O})\text{NCO}$ radical of Scheme 1 stabilizes preferentially by C-C bond fission, in which case methyl and $\text{CH}_3\text{C}(\text{O})\text{NCO}$ would be the primary products. No $\text{CH}_3\text{C}(\text{O})\text{NCO}$ was observed in the mass spectra of the chromatograms. The SAR model [49–51] predicts an OH rate constant for $\text{CH}_3\text{C}(\text{O})\text{NCO}$ of $1.0 \times 10^{-13}\text{ cm}^3\text{ molecule}^{-1}\text{ s}^{-1}$ at $T = 298$ K, so if this species is produced in the IIC + OH reaction in air, it should build up as IIC is depleted by hydroxyl radical. However, it is possible this molecule may not be stable under these conditions and may undergo further

decomposition to form small fragments, which cannot be captured on the adsorbent. Small peaks due to acetic acid and acetamide were observed as minor products, at approximately 1%–2% yield each, in the GC-MS chromatograms.

An upper bound for the tropospheric lifetime of IIC can be estimated from the weighted-average OH concentration of $9.4 \times 10^5\text{ molecules cm}^{-3}$, which has been derived for the period from 1978–2000 by Prinn et al. [57], from global measurements of methyl chloroform. Use of this value and $k_4 = 2.06 \times 10^{-12}\text{ cm}^3\text{ molecule}^{-1}\text{ s}^{-1}$ for R4 at $T = 288$ K yields a chemical lifetime of 6.0 days. The actual lifetime of IIC in the troposphere is expected to be less than this value since losses to reaction with other important oxidants such as ozone and nitrate radical are not included in this estimate. The SAR model does not predict a rate constant for reaction of IIC with ozone since IIC does not contain carbon-carbon multiple bonds. Given that rate constant information for reaction of IIC with ozone and nitrate radical is unavailable, the estimated tropospheric lifetime of IIC should be regarded strictly as an upper bound.

CONCLUSIONS

This work represents the first experimental measurement of the rate constant for the gas-phase reaction of hydroxyl radical with IIC and the first reported rate constant measurement for gas-phase reaction of any organic isocyanate with hydroxyl radical. Multi-level ab initio calculations show that three hydrogen-bonded complexes of IIC and OH occur at the reaction entrance channels. Two of these involve hydrogen

bonding to the O atom of IIC and these are connected to products via saddle points on the minimum energy paths. The third involves hydrogen bonding to the N atom of IIC. One of these (Complex 5) can proceed through subthreshold saddle point TS1 to transfer the tertiary hydrogen atom of IIC to hydroxyl radical. Conventional TST is employed to compute the rate constant for this reaction in the $T = 200\text{--}350$ K range, and with slight downward adjustment of barrier heights by 2.37 kJ mol^{-1} , theory reproduces experiment within the uncertainty. There is a small contribution to the total reaction occurring by hydrogen atom transfer from the methyl groups. The theoretical rate constants provide a basis for extrapolating the laboratory data across the range of temperature available in the troposphere. No major products of this reaction were observed; only acetic acid and acetamide were observed as minor reaction products. The tropospheric lifetime of IIC has an upper bound of 6.0 days.

SUPPORTING INFORMATION

Supporting information to this article is available at www.interscience.wiley.com. This information contains tables with equilibrium geometries, vibrational frequencies, and rotational constants for all species listed in Table II.

We thank Midwest Research Institute for support of this work. We thank Dr. Mike Schmidt of Iowa State University for a helpful discussion. We thank the reviewers of the manuscript for constructive criticisms that were helpful in our revisions.

BIBLIOGRAPHY

- Chem Eng News 1984, 62, 6–8.
- Bennet, M. *Today's Chemist at Work* 2003, April, 21–25.
- McConnell, E. E.; Bucher, J. R.; Schwetz, B. A.; Gupta, B. N.; Shelby, M. D.; Luster, M. I.; Brody, A. R.; Boorman, G. A.; Richter, C. *Environ Sci Technol* 1987, 21, 188–193.
- Atkinson, R.; Carter, W. P. L.; Winer, A. M.; Pitts, J. N. Jr. *J Air Pollut Control Assoc* 1981, 31, 1090.
- Calvert, J. G.; Atkinson, R.; Becker, K. H.; Kamens, R. M.; Seinfeld, J. H.; Wallington, T. J.; Yarwood, G. *The Mechanisms of Atmospheric Oxidation of Aromatic Hydrocarbons*; Oxford University Press: New York, 2002.
- Knispel, R.; Koch, R.; Siese, M.; Zetzsch, C. *Ber Bunsen-Ges Phys Chem* 1990, 94, 1375–1379.
- Birger, B. *J Phys Chem A* 2001, 105, 6092–6101.
- Kramp, F.; Paulson, S. E. *J Phys Chem A* 1998, 102, 2685–2690.
- Anderson, P. N.; Hites, R. A. *Environ Sci Technol* 1996, 30, 301–306.
- Atkinson, R.; Aschmann, S. M. *Int J Chem Kinet* 1989, 21, 355–365.
- Edney, E. O.; Kleindienst, T. E.; Corse, E. W. *Int J Chem Kinet* 1986, 18, 1355–1371.
- Atkinson, R.; Lloyd, A. C. *J Phys Chem Ref Data* 1984, 13, 315–444.
- Schmidt, M. W.; Baldrige, K. K.; Boatz, J. A.; Elbert, S. T.; Gordon, M. S.; Jensen, J. H.; Koseki, S.; Matsunaga, N.; Nguyen, K. A.; Su, S. J.; Windus, T. L.; Dupuis, M.; Montgomery, J. A. *J Comput Chem* 1993, 14, 1347–1363.
- Hartree, D. R. *Proc Cambridge Philos Soc* 1928, 24, 89.
- Fock, V. *Z Phys* 1930, 61, 126.
- Hall, G. G. *Proc R Soc London, A* 1951, 205, 541–552.
- Roothan, C. C. *J. Rev Mod Phys* 1951, 23, 69–89.
- Pople, J. A.; Nesbet, R. K. *J Chem Phys* 1954, 22, 571.
- McWeeny, R.; Dierksen, G. *J Chem Phys* 1968, 49, 4852.
- Ditchfield, R.; Hehre, W. J.; Pople, J. A. *J Chem Phys* 1971, 54, 724.
- Hehre, W. J.; Ditchfield, R.; Pople, J. A. *J Chem Phys* 1972, 56, 2257.
- Hariharan, P. C.; Pople, J. A. *Mol Phys* 1974, 27, 209.
- Gordon, M. S. *Chem Phys Lett* 1980, 76, 163.
- Hariharan, P. C.; Pople, J. A. *Theor Chim Acta* 1973, 28, 213.
- Blaudeau, J.-P.; McGrath, M. P.; Curtiss, L. A.; Radom, L. *J Chem Phys* 1977, 107, 5016.
- Francl, M. M.; Pietro, W. J.; Hehre, W. J.; Binkley, J. S.; DeFrees, D. J.; Pople, J. A.; Gordon, M. S. *J Chem Phys* 1982, 77, 3654.
- Binning, R. C. Jr.; Curtiss, L. A. *J Comp Chem* 1990, 11, 1206.
- Rassolov, V. A.; Pople, J. A.; Ratner, M. A.; Windus, T. L. *J Chem Phys* 1998, 109, 1223.
- Rassolov, V. A.; Ratner, M. A.; Pople, J. A.; Redfern, P. C.; Curtiss, L. A. *J Comput Chem* 2001, 22, 976.
- Moller, C.; Plesset, M. S. *Phys Rev* 1934, 46, 618.
- McLean, A. D.; Chandler, G. S. *J Chem Phys* 1980, 72, 5639.
- Krishnan, R.; Binkley, J. S.; Seeger, R.; Pople, J. A. *J Chem Phys* 1980, 72, 650.
- Clark, T.; Chandrasekhar, J.; Spitznagel, G. W.; Schleyer, P. V. R. *J Comp Chem* 1983, 4, 294.
- Frisch, M. J.; Pople, J. A.; Binkley, J. S. *J Chem Phys* 1984, 80, 3265.
- Gordon, M. S.; Truhlar, D. G. *J Am Chem Soc* 1986, 108, 5412–5419.
- Lynch, B. J.; Truhlar, D. G. *J Phys Chem A* 2003, 107, 3898–3906.
- Truong, T. N.; Truhlar, D. G. *J Chem Phys* 1990, 93, 1761–1769.
- Truong, T. N.; Truhlar, D. G. *J Chem Phys* 1992, 97, 8820.
- Lynch, B. J.; Zhao, Y.; Truhlar, D. G. *J Phys Chem A* 2005, 109, 1643–1649.

40. Zheng, J.; Zhao, Y.; Truhlar, D. G. *J Chem Theory Comput* 2007, 3, 569–582.
41. Eyring, H. *J Chem Phys* 1935, 3, 107.
42. Evans, M. G.; Polyani, M. *Trans Faraday Soc* 1935, 31, 875.
43. Truhlar, D. G.; Isaacson, A. D.; Garrett, B. G. In *Theory of Chemical Reaction Dynamics*; Baer, M. (Ed.); CRC Press, Inc.: Boca Raton, FL, 1985; Vol. 4.
44. Eckart, C. *Phys Rev* 1930, 35, 1303–1309.
45. Atkins, P.; de Paula, J. *Physical Chemistry*, 7th ed.; W. H. Freeman and Company: New York, 2002.
46. Merrick, J. P.; Moran, D.; Radom, L. *J Phys Chem A* 2007, 111, 11683–11700.
47. Lynch, B. J.; Fast, P. L.; Harris, M.; Truhlar, D. G. *J Phys Chem A* 2000, 104, 4811.
48. Atkinson, R.; Arey, J. *Chem Rev* 2003, 103, 4605–4638.
49. Atkinson, R. *Chem Rev* 1986, 86, 69–201.
50. Atkinson, R. *Int J Chem Kinet* 1987, 19, 799–828.
51. Kwok, E. S. C.; Atkinson, R. *Atmos Environ* 1995, 29, 1685–1695.
52. Flükiger, P.; Lüthi, H. P.; Portmann, S.; Weber, J. *MOLEKEL 4.3*; Swiss National Supercomputing Centre CSCS: Manno (Switzerland), 2000.
53. Ishida, K.; Morokuma, K.; Komornicki, A. *J Chem Phys* 1977, 66, 2153–2156.
54. Smith, I. W. M.; Ravishankara, A. R. *J Phys Chem A* 2002, 106, 4798–4807.
55. Chuang, Y.-Y.; Truhlar, D. G. *J Chem Phys* 2000, 112, 1221–1228.
56. Finlayson-Pitts, B. J.; Pitts, J. N., Jr.; *Chemistry of the Upper and Lower Atmosphere*; Academic Press; San Diego, CA, 2000.
57. Prinn, R. G.; Huang, J.; Weiss, R. F.; Cunnold, D. M.; Fraser, P. J.; Simmons, P. G.; McCulloch, A.; Harth, C.; Salameh, P.; O'Doherty, S.; Wang, R. H. J.; Porter, L.; Miller, B. R. *Science* 2001, 292, 1882–1888.